ACS APPLIED MATERIALS & INTERFACES

Research Article

www.acsami.org

Design and Fabrication of a Thin-Walled Free-Form Scaffold on the Basis of Medical Image Data and a 3D Printed Template: Its Potential Use in Bile Duct Regeneration

Suk-Hee Park,[†,▽] Bo-Kyeong Kang,[‡,▽] Ji Eun Lee,[†] Seung Woo Chun,[†] Kiseok Jang,[§] Youn Hwan Kim,[∥] Mi Ae Jeong,[⊥] Yohan Kim,[#] Kyojin Kang,[#] Nak Kyu Lee,[†] Dongho Choi,[*,#] and Han Joon Kim[*,#]

[†]Micro/Nano Scale Manufacturing R&D Group, Korea Institute of Industrial Technology, Ansan-si, Gyeonggi-do 426-910, Korea
[‡]Department of Radiology, [§]Department of Pathology, [∥]Department of Plastic and Reconstructive Surgery, [⊥]Department of Anesthesiology and Pain Medicine, and [#]Department of Surgery, College of Medicine, Hanyang University, 222 Wangsimri-ro, Seongdonggu, Seoul 04763, Korea

ABSTRACT: Three-dimensional (3D) printing, combined with medical imaging technologies, such as computed tomography and magnetic resonance imaging (MRI), has shown a great potential in patient-specific tissue regeneration. Here, we successfully fabricated an ultrathin tubular free-form structure with a wall thickness of several tens of micrometers that is capable of providing sufficient mechanical flexibility. Such a thin geometry cannot easily be achieved by 3D printing alone; therefore, it was realized through a serial combination of processes, including the 3D printing of a sacrificial template, the dip coating of the biomaterial, and the removal of the inner template. We demonstrated the feasibility of this novel tissue engineering construct by conducting bile duct surgery on rabbits. Moving from a rational design based on MRI data to a successful surgical procedure for reconstruction, we confirmed that the presented method of fabricating scaffolds has the potential for use in customized bile duct regeneration. In addition to the specific application presented here, the developed process and scaffold are expected to have universal applicability in other soft-tissue engineering fields, particularly those involving vascular, airway, and abdominal tubular tissues.

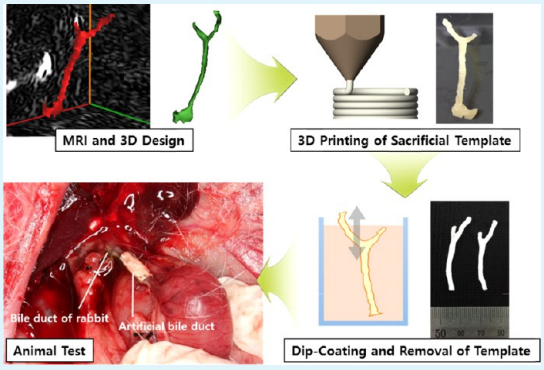

KEYWORDS: *3D printing, dip coating, medical imaging, customized scaffold, bile duct reconstruction*

1. INTRODUCTION

Recent advances in three-dimensional (3D) printing technology have led to the development of a number of advantageous applications in the manufacturing of customized consumer and industrial products. Throughout biomedical fields, 3D printing has been exploited to fabricate various rapidly prototyped devices, such as visual aids,[1] surgical tools,[2] biocompatible prostheses,[3] and tissue engineering scaffolds.[4,5] Scaffold-based strategies are among the most effective methods for tissue regeneration, and they have been developed by using several types of 3D printing techniques, including photopolymerization,[6,7] material extrusion (ME),[8,9] and powder fusion or binding methods.[10,11] Of the proposed processes, direct nozzle-based printing approaches, such as ME, have been preferred by most researchers for scaffold fabrication, owing to the diversity of available materials, including FDA-approved polymers, functional biochemicals, and even living cells.[12,13]

Although the nozzle-based 3D printing technique has been used to achieve a wide range of striking bioapplicable constructs, it presents limitations in the implementation of minimum geometries. The minimum diameters of commercial nozzles typically range from approximately one hundred to several hundreds of micrometers, and the nozzles with smaller diameters require specialized processes with higher costs. Besides the cost issue, a much higher driving pressure must be exerted on polymer melts when 3D printing nozzles of smaller diameters are used, to achieve continuous extrusion at the nozzle tip.[14,15] The necessarily required huge pressure produces a polymer melt extrusion that is hard, slow, and unstable.[16] The difficulty in realizing a small feature size, particularly below 100 μm, restricts the mechanical flexibility of the printed construct despite the use of soft rubberlike materials. Undoubtedly, the mechanical properties of the scaffold should be consistent with those of the target tissue to prevent physical inflammation in adjacent tissues after scaffold transplantation.[4,17−19] Given the high mechanical compliance and flexibility of soft tissues in the human body, scaffolds for such tissue should be designed as easily deformable architectures.

Here, we introduce a comprehensive approach for the application of 3D printing to the arbitrary shaping of a flexible

Received: January 17, 2017
Accepted: March 21, 2017
Published: March 21, 2017

DOI: 10.1021/acsami.7b00849
ACS Appl. Mater. Interfaces 2017, 9, 12290−12298

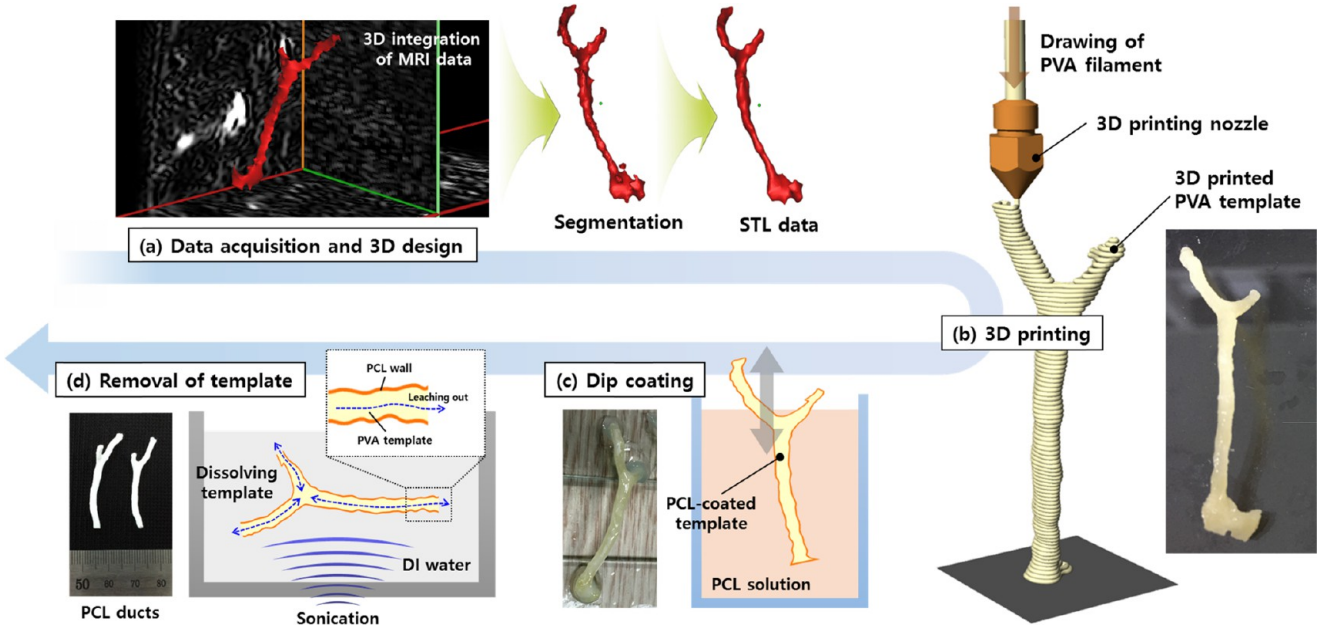

Figure 1. Schematic illustration with photos of the overall fabrication procedure from data acquisition to postprocessing. (a) Modeling of the 3D target structure in STL format on the basis of medical image data. (b) 3D printing of the PVA sacrificial template structure using the ME technique. (c) Dip coating of PCL and the formation of a thin film over the PVA template. (d) Removal of the core PVA template by dissolution in water under sonication.

tubular scaffold. Our method involves 3D design, 3D printing, postprocessing, and animal experimentation. Planar images acquired from computed tomography (CT) or magnetic resonance imaging (MRI) were processed and built into 3D object data of the target tissue. According to the designed geometry, a sacrificial template was fabricated through a 3D printing process using a water-soluble material. The 3D template was dip-coated with a solution of biomaterial, and a thin film was deposited on the template. After the sacrificial template was removed by water, the surrounding film was leached as a thin-wall tubular structure. Because of the small thickness, within the range of several tens of micrometers, the fabricated tubular structures exhibited a much enhanced mechanical flexibility compared to that of the directly 3D-printed structures with wall thicknesses of over hundreds of micrometers. Because of its high flexibility and biocompatibility, our engineered scaffold could be used in the construction of an artificial bile duct.

According to the demands of hepatobiliary surgery, artificial bile ducts may be required in cases of postoperative bile duct injury, biliary strictures, malignancies, and liver transplantation.[20] Bile duct resection and bilo-enteric anastomosis have been used in such situations; however, long-term follow-up studies of biliary-enteric bypass have indicated a relatively high incidence of anastomosis stricture and retrograde cholangitis.[21] Artificial bile ducts constructed from appropriate materials that can fit perfectly in the original 3D space can be used in complicated biliary surgery. Our developed scaffold, which was designed and tailor-made according to the magnetic resonance cholangiopancreatography (MRCP) of a rabbit, was transplanted into an injured bile duct, and its functionality was confirmed. The geometric advantages of this technique, such as the customized three dimensionality and microscale wall thickness, are not limited to any specific tissue and would allow for a wide range of feasible applications in scaffold-based tissue regeneration.

2. MATERIALS AND METHODS

2.1. MRI Examination and 3D Design of the Target Tissue. MRI was performed 1 day before surgery and 3 days after surgery in the tested rabbits. All MRI examinations were performed on a 3-T MR scanner (Ingenia; Philips Healthcare, Best, the Netherlands) using a small extremity coil. Each rabbit was anesthetized with intramuscular ketamine (40−100 mg/kg) and xylazine (5−13 mg/kg) during the MRI scan. After a three-plane localization imaging gradient echo sequence was obtained, respiratory-triggered 3D MRCP images and thick-slab single-shot 2D MRCP images were obtained. The following sequence parameters were used: repetition time, 1044 ms; echo time, 650 ms; acquisition time, 2−3 min; flip angle, 90°; slice thickness, 1 mm (no gap); field of view, 200 × 200 mm^2; and matrix for 3D MRCP, 200 × 200. The acquired 3D MRCP images, which were saved in the digital imaging and communications in medicine (DICOM) format, were processed into a 3D object in a 3D-printable file format (STL, surface tessellation language) using commercial software (Mimics; Materialise, Louvain, Belgium).

2.2. Fabrication of the Thin-Wall Tubular Scaffold. The procedures for the scaffold fabrication included the 3D printing of the template, the dip coating of the biomaterial and the removal of the template. For the 3D printing of the sacrificial template, commercial water-soluble filaments of poly(vinyl alcohol) (PVA Filament; ESUN, China) with a diameter of 1.75 mm were loaded and fed into an ME-based 3D printer. The printing system was a homemade machine built on the basis of RepRap Mendel 3D printer. It included one and three stepping motors, respectively, for ME and $x-y-z$ motion of printing components, which were controlled by Arduino microcontroller. The open-source software, Cura, was used for the generation of G-code and process parameters. The templates were 3D-printed with a nozzle with an inner diameter of 0.25 mm and a heating temperature of 170 °C. The layer thickness for the 3D printing was set to 0.1 or 0.15 mm. To enhance the surface quality, the printed parts were immersed and sonicated in warm distilled water at 50 °C for 1 min so that the surface roughness could be smoothed by redissolving the bumpy and uneven surface of the printed parts. The surface roughness of the specimen was measured by a commercial profilometer (Rugosurf 90G, Hexagon Metrology).

After the smoothed part was dried, it was dipped into a solution of polycaprolactone (PCL, MW 80 000; Sigma-Aldrich, MO) dissolved in

DOI: 10.1021/acsami.7b00849
ACS Appl. Mater. Interfaces 2017, 9, 12290−12298

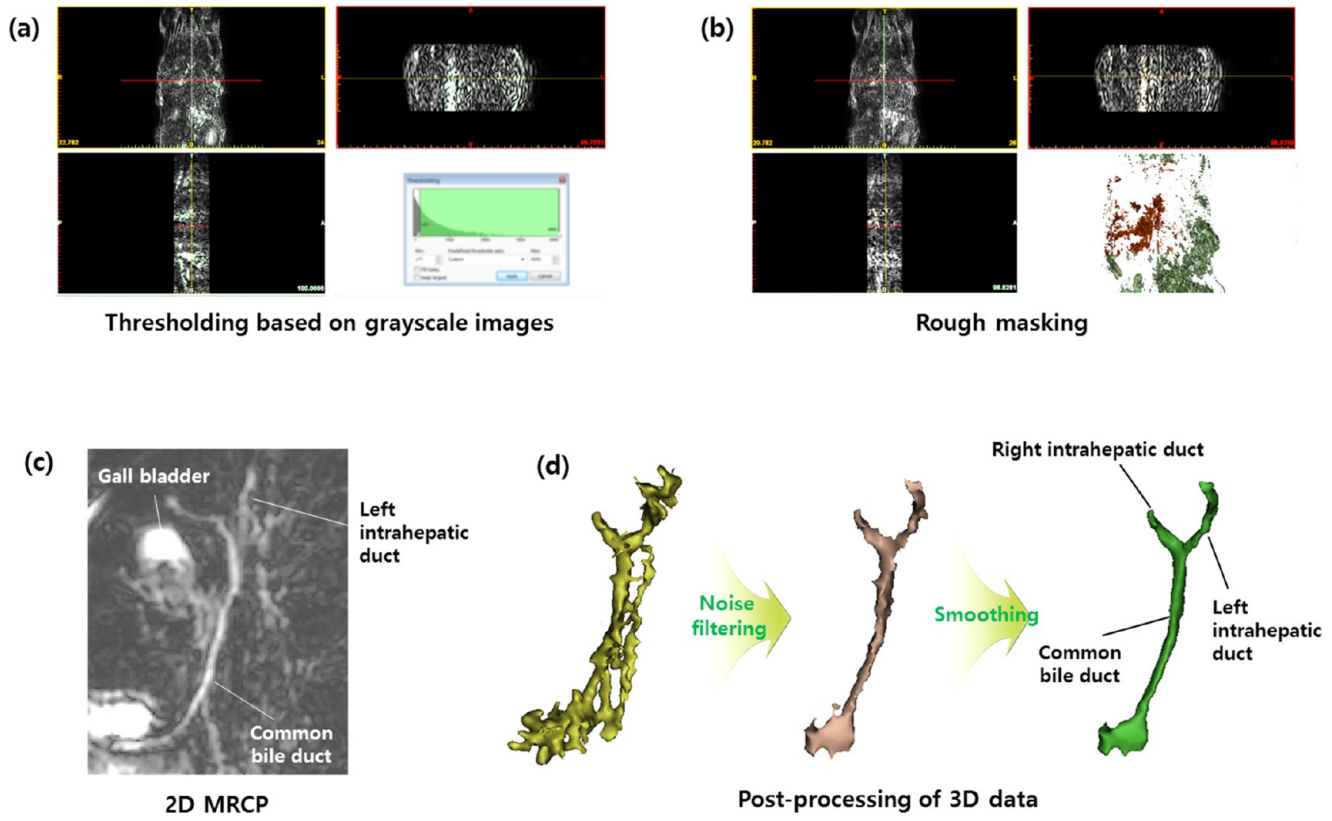

Figure 2. Generation of 3D object data for 3D printing from MRI data. (a) Selection of target region by adaptive thresholding of grayscale MRCP image data. (b) Cropping of the target region (bile duct) by masking and excluding unnecessary areas. (c) 2D MRCP image used as the reference in the 3D reconstruction. (d) Final development of the 3D data of the bile duct via noise filtering and smoothing.

dichloromethane (Samchun Pure Chemical, Korea) at concentrations of 10, 15, and 20% (w/v). The solution concentration was varied to modulate the thickness of the dip-coated film. As the solvent evaporated, a solid film of PCL was formed on the surface of the PVA template. Then, the PCL-coated PVA part was immersed again into distilled water, thereby removing the core sacrificial PVA template. Because the dip-coated part was completely covered with the PCL film, the small end of the part was cut before the immersion to secure an entrance for water penetration in the template removal process. By exerting sonication with 40 kHz in warm water at 50 °C for up to 45 min, the PVA template could be completely removed, and the surrounding PCL film was left as a tubular form. Before the animal surgery, the tubular scaffold was dried and sterilized overnight under ultraviolet irradiation.

2.3. Animal Experiments. The animal experiments were performed with the permission of the Institutional Animal Care and Use Committee (IACUC) of Hanyang University. All experiments were performed in compliance with NIH guidelines and Hanyang University's animal research protocol. Male semispecific pathogen-free rabbits at 21 months of age weighing 3−4 kg were used in this study. All animals were housed under standard conditions for a 12 h light/dark cycle and fed a standard diet during an adaptation period of over 4 weeks, and they were fasted for 12 h before surgery. Under general anesthesia administered by an anesthesiologist, the animals were immobilized in the supine position and laparotomized via a midline incision in the upper abdomen to expose the extrahepatic bile duct (EHBD). The lower EHBD was transected, and the artificial bile duct was anastomosed end-to-end to the proximal and distal ends of the EHBD with interrupted 10−0 Ethilon sutures under light microscopy.[22] All anastomosis was performed by a microsurgeon, and we confirmed adequate bile drainage through the anastomosed artificial bile duct during the surgery. After the procedure, the abdominal cavity was irrigated with warm saline and closed. For the histological analysis, fresh tissues obtained from the rabbit liver and bile duct with the artificial bile duct were immediately fixed in 10% neutral buffered formalin. After 24 h of fixation, the tissues were processed, embedded in paraffin, sectioned at 4 μm, and stained with hematoxylin and eosin (H&E). Histopathologic examinations of the bile duct and liver sections were conducted by a pathologist.

3. RESULTS AND DISCUSSION

3.1. 3D Design Process of the Target Tissue. Figure 1 illustrates the procedures used for fabricating a customized tubular scaffold characterized by a patient-specific arbitrary shape, a low wall thickness, and an adequate mechanical flexibility. The engineering of customized medical device using 3D printing requires a comprehensive approach involving 3D design (Figure 1a), 3D printing (Figure 1b), and postprocessing (Figure 1c,d). The custom scaffold was achieved through a coordination between modeling and manufacturing, by using computer-aided design (CAD) and 3D printing techniques. The 3D design process was conducted using medical image data. In this article, we started from the data processing of the 3D MRCP, fabricated the net-shaped tubular scaffolds, and applied the scaffolds in bile duct regeneration. The commercial software Mimics allowed a rough 3D reconstruction from 2D DICOM images through built-in functions, such as thresholding and masking, as shown in Figure 2a,b. For the fine development of the reconstruction on the basis of 3D object data, 2D MRCP images were used as a reference (Figure 2c). A radiologist (with 5 years of experience in MRCP) excluded intestinal fluid, renal pelvises and ureters, the spinal cord, and other artifacts from the reconstructed image (Figure 2d). Considering practicality in scaffold-based operation, in which surgeons occasionally must cut out the prepared scaffold for

DOI: 10.1021/acsami.7b00849
ACS Appl. Mater. Interfaces 2017, 9, 12290−12298

necessary clinical circumstances, we designed and fabricated a whole anatomical structure of a bile duct system composed of a common bile duct and right and left intrahepatic ducts. Such realistic and integrative features are distinct from those of previous artificial bile ducts, which have had only primitive cylindrical shapes,[22−24] and can be used to plan and conduct clinical surgeries with greater freedom and accuracy.

3.2. 3D-Printed Sacrificial Template. We utilized a 3D printing technique for the net-shaping of the designed scaffold. The printed construct was used as a sacrificial template for thin-film formation in the subsequent dip-coating step. Because the geometry of the final thin tubular scaffold depended on the geometry of the printed template, the 3D printing process needed to be carefully controlled. The ME process is one of the most universal and reliable 3D printing techniques in terms of the versatility of materials. Most thermoplastic polymers can be processed into the 3D-printed construct under optimized process parameters, including the flow geometry, the heating condition, and the moving speed of the nozzle.[25,26] Among the various thermoplastic biocompatible polymers, PVA has a great water solubility, which increases its suitability for use as the sacrificial template.[27−29] As shown in Figure 1b, the PVA template was successfully fabricated according to the 3D design data. The geometric features of the 3D-printed structures, particularly with ME, are typically dependent on the layering process parameters of the material deposition, such as the layering direction and thickness. The paths for the 3D printing were generated according to the layering direction, which was determined in a longitudinal manner with reference to the overall morphology of the designed structure. In addition to the well-ordered printing paths, the close-layering deposition at a thickness of 0.15 mm formed a defect-free 3D construct as shown in the inset of Figure 1b. When the layering thickness was set over 0.2 mm, failures and defects occurred during printing regions with steep branch parts (hepatic and cystic ducts in our example). Because our target shape was a tubular structure for an artificial bile duct, the accuracy of the cross-sectional geometry was important for suturing to the surgical site of the bile duct. To quantify the printing accuracy, circular features with different diameters were printed as shown in Figure 3a−c. The diameters of the actual printed structures did not show significant differences from the diameters in the original CAD data, as shown in Figure 3d. The printed structures with diameters of 1, 2, and 6 mm had error ranges of less than 5% from each target. Because of the minimum dimension limits of the printed strand, which are generally determined by the printing nozzle diameter, precise sub-millimeter dimensions could not easily be realized by using the typical nozzle, which has a 0.25 mm diameter. For the 0.6 mm diameter cylinder, relatively large errors that could exceed 25% were observed between the design and measured data. For smaller features, we are planning to develop a deposition system with enhanced accuracy for 3D printing, including smaller-diameter nozzles and more dilute materials.

Although the layer thicknesses of the printed structure were reduced to 0.15 and 0.1 mm, the surface roughnesses in R_{max} remained at approximately 52 and 37 μm, respectively. These values could not be ignored because the thickness of the dip-coated biomaterial in the following step was less than 100 μm. The rugged surface of the sacrificial template would be naturally transferred onto the dip-coated biomaterial film and might cause defects or mechanical weakness in the final tubular structure and interrupt the flow of body fluid inside the tube

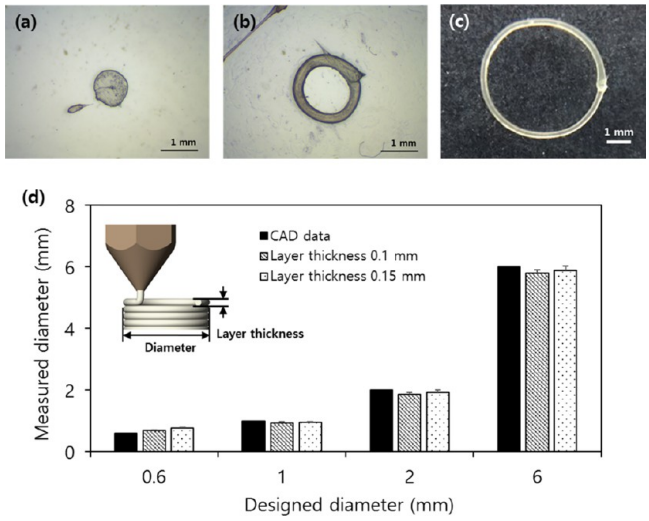

Figure 3. Circular printed PVA structures with different diameters of (a) 1 mm, (b) 2 mm, and (c) 6 mm. (d) Comparison of the measured diameters of the 3D-printed cylinders with reference to the diameter of the original designed geometry. The diameter of the 3D-printed cylinder varied (1, 2, and 6 mm). Data are shown as mean ± standard deviation (n = 15).

after transplantation. To overcome these problems, we performed a dip-smoothing process, as shown in Figure 4a. The printed structure was immersed in warm water at 50 °C for 1 min with gentle sonication. Cross-sectional images of the printed PVA structures before and after the dip-smoothing process are shown in Figure 4b,c, respectively. The rugged surface was slightly redissolved in water and smoothed. The smoothing effect was confirmed by the reduced R_{max} of 9 and 8 μm for the specimens printed at layer thicknesses of 0.1 and 0.15 mm, as shown in Figure 4d,e, respectively. The periodic but relatively large fluctuation on each surface was alleviated to form an even profile. The surface of the sacrificial template was smoothed to ensure an even deposition of the biomaterials in the subsequent dip-coating procedure, thereby achieving a favorable tubular structure with a uniform wall thickness in the final step.

3.3. Characterization of Thin-Wall Tubular Scaffold. As shown in Figure 1c, the 3D-printed and surface-smoothed PVA template was dipped into PCL solution. As the solvent evaporated from the solution, a thin film surrounding the template was deposited in the solid state. In the typical dip-coating procedure, the thickness of the coated film is influenced by the concentration of the dipping solution because of simple fluid dynamics.[30] Our method using the water-soluble template for dip coating confirmed the feasibility of thin-film formation as other previous works using insoluble mold.[31] As shown in Figure 5a, a solution with a lower concentration resulted in the deposition of a smaller thickness of material. When the solution was diluted to a concentration of 10% (w/v), the average thickness of the film was reduced to 33 μm. After removal of the inner PVA template, this thin-wall tube was easily torn and showed holes and cracks, which might cause critical bile leakages. Considering the requirements for the structural stability and flexibility, we chose the intermediate condition of 15% (w/v), which yielded a tubular construct with a wall thickness of approximately 60 μm.

The 3D-printed PVA template covered in the coated PCL film was finally removed by dissolution in deionized water. For

DOI: 10.1021/acsami.7b00849
ACS Appl. Mater. Interfaces 2017, 9, 12290−12298

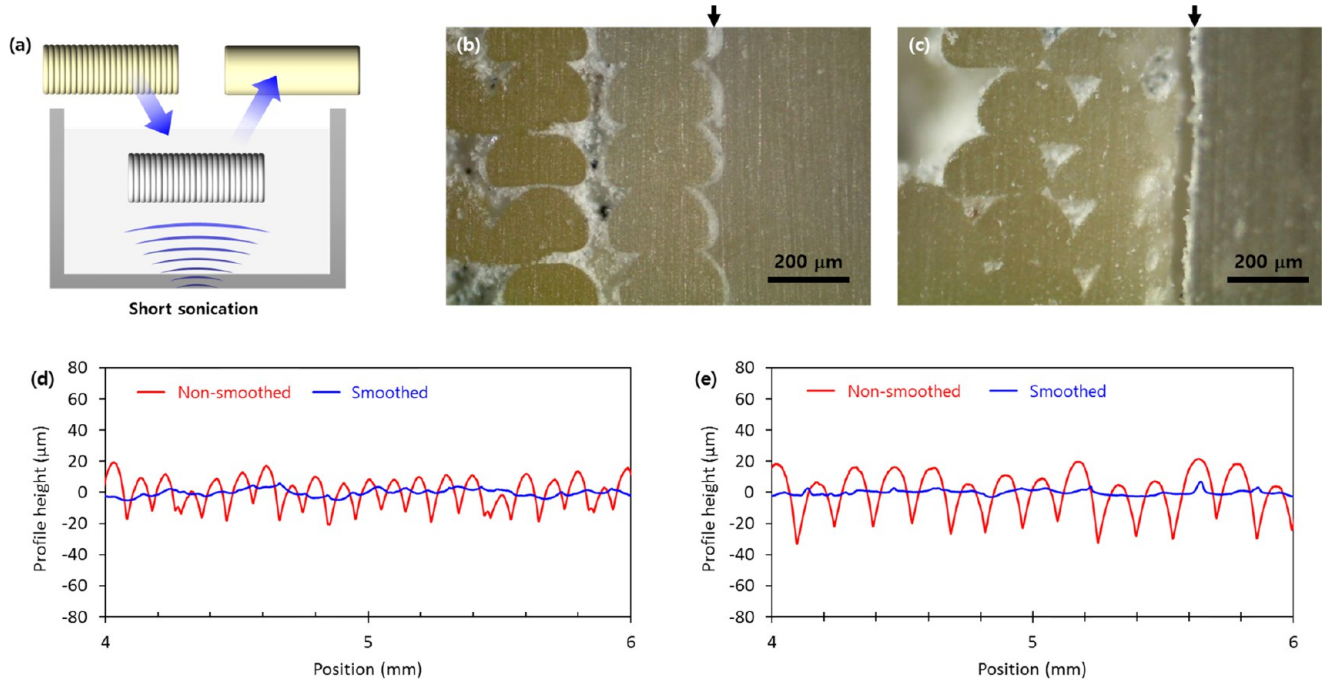

Figure 4. (a) Schematic illustration of the dip-smoothing process of the 3D-printed PVA sacrificial templates. Microscopic cross-sectional images of (b) nonsmoothed and (c) smoothed PVA structures. Each arrow in (b) and (c) indicates the boundary of the PVA structure. The images in (b) and (c) are at the same magnification. Surface profile changes of the 3D-printed structures with layer thicknesses of (d) 0.1 mm and (e) 0.15 mm before and after the smoothing process.

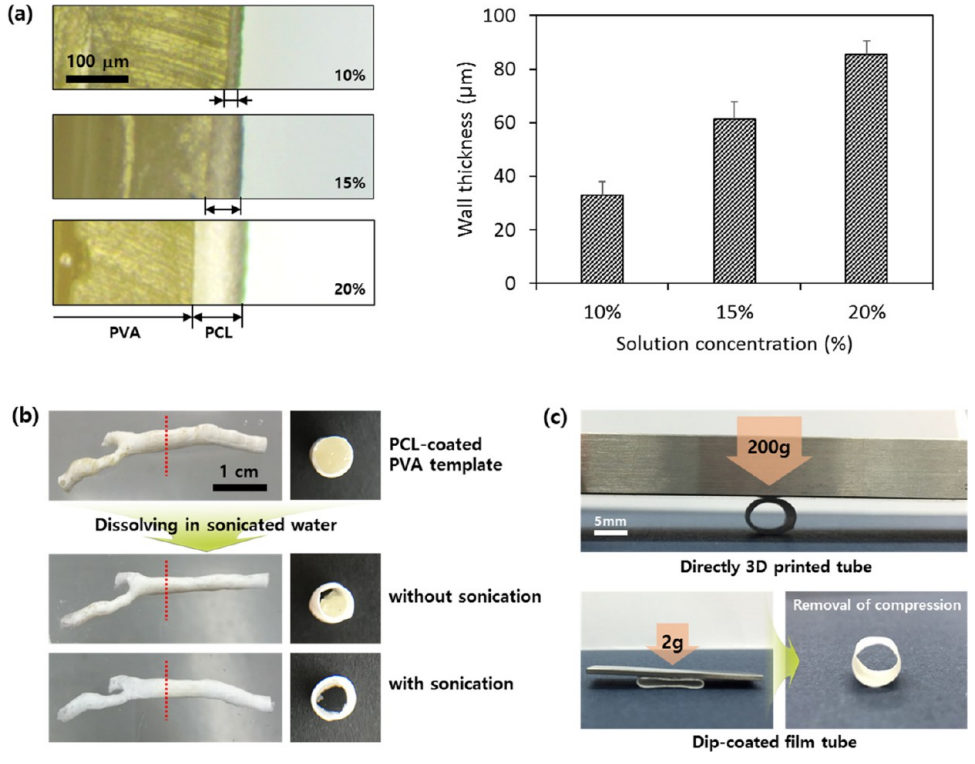

Figure 5. (a) Microscopic images and quantitative thickness data of the PCL film deposited by the dip-coating process. The solution concentrations for the dip coating were 10, 15, and 20% (w/v). The data in the histogram are shown as mean ± standard deviation (n = 5). (b) Dissolution and removal of the inner PVA template by sonication in distilled water. (c) Compression tests using a directly 3D-printed tube and a dip-coated film tube.

the efficient dissolution and removal of the PVA, the water was heated to 50 °C, which is slightly lower than the melting point of PCL (60 °C). After 45 min, we confirmed that the PVA was entirely removed as shown in Figure 5b. From this experimental procedure, we determined that sonication was a critical factor for the template removal process. For our target

DOI: 10.1021/acsami.7b00849
ACS Appl. Mater. Interfaces 2017, 9, 12290−12298

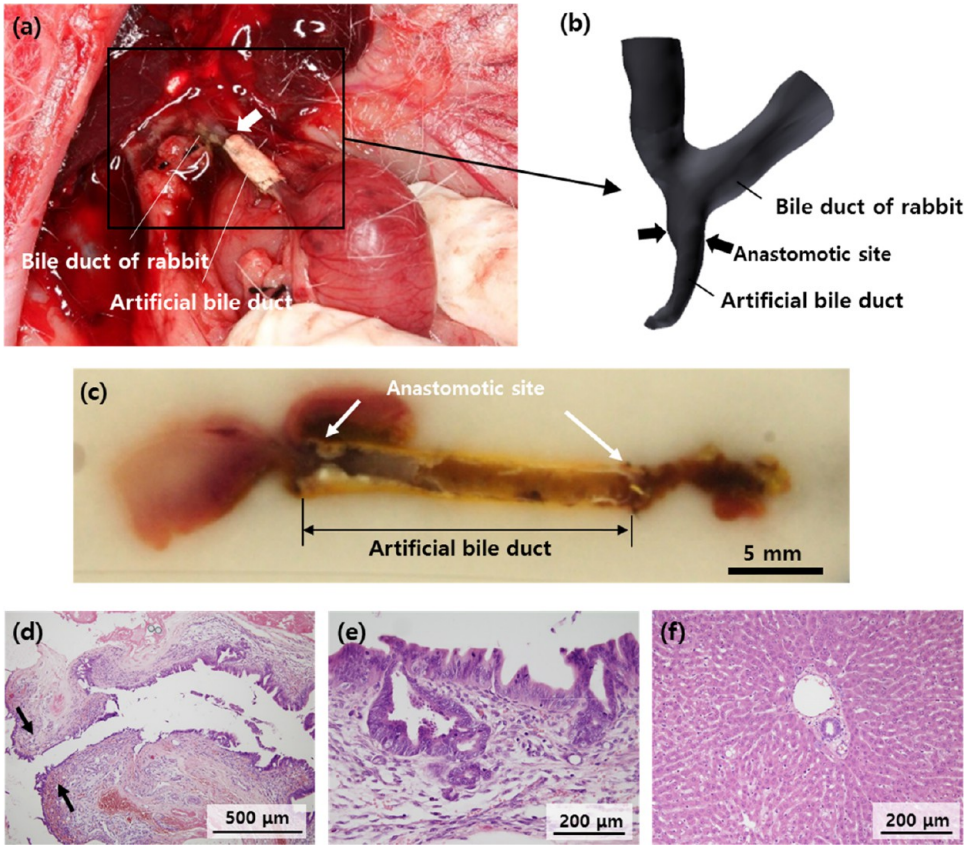

Figure 6. (a) Photograph of the anastomosed bile duct. (b) 3D-reconstructed MRCP image shows the anastomotic site and both dilated intrahepatic bile ducts of the rabbit. The 3D reconstruction was processed by the same manner as Figure 2. (c) Photograph of the sectioned tissue containing the replaced artificial bile duct. Histopathological examination of the rabbit bile duct and liver. (d) Bile duct wall adjacent to the anastomosis site (black arrows). (e) Mucosal epithelium inside the bile duct wall showing normal regenerative atypia. (f) Liver parenchyma with well-preserved hepatic lobules and portal area.

shape, which was relatively narrow and had a branched morphology, the core template materials were not totally removed if sonication was not applied (Figure 5b). The sonicated water completely dissolved and removed the PVA materials, thereby leaving a clear hollow tube of PCL. Because of the optimal PCL film thickness set in the dip-coating step, defects were not observed in the developed tube construct, and sufficient mechanical flexibility was maintained. We used PCL as the component biomaterial of the final scaffold. Because of its extremely low glass-transition temperature (−60 °C), the PCL-based structure exhibited a rubberlike material behavior at room temperature. Together with the thin-wall geometry at the micrometer scale, the favorable material properties were able to synergistically achieve a sufficient level of flexibility when used as a soft-tissue scaffold. The synergistic advantage was demonstrated in a simple compression test that compared the dip-coated film tube with a directly 3D-printed tube (Figure 5c). Using a homemade PCL filament, we printed a tube-shaped cylinder with wall thickness ranging from 500 to 600 μm, which is the typical width of a single strand deposited in the ME process. As shown in Figure 5c, limited deformations were observed in the relatively thick-walled tube when 200 g of the compressive force was exerted in the radial direction. Compared with the stiffness of thick-walled tubes, dip-coated tubes with a wall thickness of less than 100 μm exhibited a high compliance, large deformations under a much smaller force of 2 g, and a better structural resilience thereafter. We expect that a superior mechanical flexibility would be advantageous for the functioning of engineered scaffolds used for the regeneration of soft tissues, including our target bile duct.

3.4. Feasibility Test during Animal Surgery. The feasibility of the developed tubular structure was tested via rabbit surgery. An approximately 10 mm long part of the common bile duct was excised from the native rabbit bile duct and replaced with a partial artificial duct cut from the whole entity as shown in Figures 1d and 5b. Because of the similarity between the artificial and native ducts, a region could be easily determined in an identical location to that of the excised tissue. The cutting and suturing of the artificial bile duct were easily performed because of the softness of the material, and an appropriate length of bile duct was easily separated from the total length of the manufactured bile duct, which was well fit as an anatomical structure. Because the surgical knots were compatible with the elasticity and flexibility of the component material (PCL), we did not observe bile leakage at the anastomotic site during surgery.

Three days after the surgery, MRI was performed again on the surviving rabbit. As shown in Figure 6b, the 3D-reconstructed MRCP image demonstrated that the anastomotic site provided a smooth interconnection between the native and artificial bile ducts and was well preserved without bile leakage. The 3D MRCP image also showed a mild dilatation of both intrahepatic ducts because of an anastomotic stricture. Despite the slight stricture, the MRCP image revealed a sound bile flow across the anastomotic site without any blockage or leakage. After the MRI observations, the animal was sacrificed and

DOI: 10.1021/acsami.7b00849
ACS Appl. Mater. Interfaces 2017, 9, 12290−12298

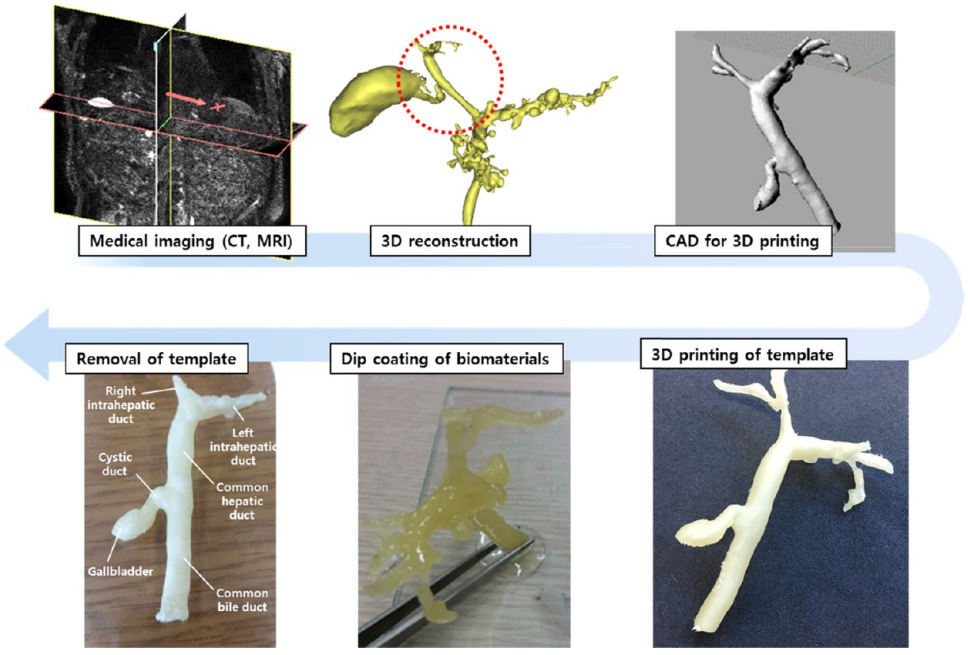

Figure 7. Potential application in clinical surgery for bile duct regeneration. 3D volumetric MRCP data were obtained using 3T-MRI with respiratory gating from a patient with chronic abdominal pain. Detailed anatomical structures of the biliary tree are shown in the final processed artificial bile duct, including hepatic and cystic ducts (the leftmost image in the second row).

autopsy was performed. In the intra-abdominal approach and in the MRI, we confirmed that the bile leakage was minimal, and the integrity of the suture between the native bile duct and artificial bile duct was maintained. In addition, mismatches were not observed between the original bile duct and the artificial bile duct.

A histological analysis was performed on an extracted tissue construct containing the replaced artificial bile duct (Figure 6c) by staining the surgically treated bile duct and liver parenchyma with hematoxylin and eosin (H&E). As shown in Figure 6d,e, the histopathologic examination of the anastomosis site of the bile duct revealed an appropriate healing process after the surgery. The wall of the bile duct was slightly thickened and showed epithelial regenerative changes, a mild lymphocyte infiltration, and a minimal fibroblastic proliferation with no evidence of bile leakage into the surrounding tissue (Figure 6d). No foreign-body reactions or destructive inflammatory changes were observed. As shown in Figure 6e, the mucosal epithelium exhibited a normal regenerative process. In addition, the liver parenchyma was well preserved, and the histologic evidence of bile duct obstruction was not observed (Figure 6f).

In a small animal model, such as the rabbit model in this experiment, only the common bile duct could be reconstructed because of the limited minimal printing diameter of 1 mm. However, in the case of a large animal or human, for which the diameters of the bile ducts are in the range of several millimeters,[32] the developed artificial duct would be feasible, on the basis of the resolution of 3D printing. Figure 7 shows that the presented approach has the potential for use in clinical applications. MRI data were obtained from a patient with an intraductal papillary mucinous neoplasm in the pancreas, and a 3D image was reconstructed on the basis of these data and then processed as an artificial bile duct according to our fabrication procedures. The 3D image showed a normal biliary tree and multiple cystic lesions (intraductal papillary mucinous neoplasm, branch duct type) along the main pancreatic duct. On the basis of the processed CAD data, the as-fabricated artificial bile duct exhibited most of the confluent portions and second-order branches, such as the hepatic and cystic ducts. The detailed geometry of the artificial construct, including the lesion site, is expected to provide superior functions for patient-specific bile duct surgery compared with the conventional cylindrical duct, which has a primitive shape of single trunk. The goal of this study was to produce an anatomically well-fitted artificial bile duct. Previously, a long-term survival study showed that a tubular space surrounded by inflammatory cells and connective tissue was formed.[22] The epithelialization of the transplanted artificial bile duct has also been reported in experiments using basic fibroblast growth factor[33] and human mesenchymal stem cells.[34] To determine the degree of epithelialization and the long-term survival, we are planning further studies using the developed artificial bile ducts covered with cultures of growth factors and cells.

4. CONCLUSIONS

To formulate a net-shaped construct customized from CAD data based on CT or MRI, we utilized 3D printing techniques combined with a biomaterial dip-coating process. Our method could produce thin-wall tubular structures with thicknesses less than 100 μm. Compared with conventionally 3D-printed tubes, the structures produced using our technique provided a superior flexibility without impairments in the geometric integrity of the 3D structure. In an animal experiment involving bile duct regeneration, the tailored shape of the artificial duct demonstrated feasibility and usefulness in practical surgery. In addition, the histological results indicated the potential of this method for use in bile duct regeneration. The advantages of our developed method, which is capable of delivering customizability, three dimensionality, mechanical flexibility, and biocompatibility, suggest that it has the potential to meet the needs of practical tissue engineering applications.

DOI: 10.1021/acsami.7b00849
ACS Appl. Mater. Interfaces 2017, 9, 12290−12298

AUTHOR INFORMATION

Corresponding Authors

*E-mail: crane87@hanyang.ac.kr. Tel: +82-2-2220-8449. Fax: +82-2-2281-0224 (D.C.).

*E-mail: thicknyh@gmail.com. Tel: +82-31-560-2043. Fax: +82-31-566-4409 (H.J.K.).

ORCID

Suk-Hee Park: 0000-0002-5515-8660

Author Contributions

▽S.-H.P. and B.-K.K. equally contributed to this work.

Notes

The authors declare no competing financial interest.

ACKNOWLEDGMENTS

This work was supported by the Industrial Fundamental Technology Development Program funded by the Ministry of Trade, Industry and Energy (MOTIE) of Korea (10051680, Development of high strength and environmental friendly polymer for 3D printing), a KITECH (Korea Institute of Industrial Technology) internal project, and the Technology Innovation Program or Industrial Strategic Technology Development Program (10063334, Vascularized 3D tissue (liver/heart, cancer) chip for evaluation of drug efficacy and toxicity) funded by the MOTIE.

REFERENCES

(1) McGurk, M.; Amis, A. A.; Potamianos, P.; Goodger, N. M. Rapid Prototyping Techniques for Anatomical Modelling in Medicine. *Ann. R. Coll. Surg. Engl.* **1997**, *79*, 169−174.

(2) Giacomo, G. A. P. D.; Cury, P. R.; de Araujo, N. S.; Sendyk, W. R.; Sendyk, C. L. Clinical Application of Stereolithographic Surgical Guides for Implant Placement: Preliminary Results. *J. Periodontol.* **2005**, *76*, 503−507.

(3) Dai, K. R.; Yan, M. N.; Zhu, Z. A.; Sun, Y. H. Computer-Aided Custom-Made Hemipelvic Prosthesis Used in Extensive Pelvic Lesions. *J. Arthroplasty* **2007**, *22*, 981−986.

(4) Hollister, S. J. Porous Scaffold Design for Tissue Engineering. *Nat. Mater.* **2005**, *4*, 518−524.

(5) Hutmacher, D. W.; Sittinger, M.; Risbud, M. V. Scaffold-Based Tissue Engineering: Rationale for Computer-Aided Design and Solid Free-Form Fabrication Systems. *Trends Biotechnol.* **2004**, *22*, 354−362.

(6) Cooke, M. N.; Fisher, J. P.; Dean, D.; Rimnac, C.; Mikos, A. G. Use of Stereolithography to Manufacture Critical-Sized 3D Biodegradable Scaffolds for Bone Ingrowth. *J. Biomed. Mater. Res., Part B* **2003**, *64*, 65−69.

(7) Lee, K. W.; Wang, S. F.; Fox, B. C.; Ritman, E. L.; Yaszemski, M. J.; Lu, L. C. Poly(propylene fumarate) Bone Tissue Engineering Scaffold Fabrication Using Stereolithography: Effects of Resin Formulations and Laser Parameters. *Biomacromolecules* **2007**, *8*, 1077−1084.

(8) Zein, I.; Hutmacher, D. W.; Tan, K. C.; Teoh, S. H. Fused Deposition Modeling of Novel Scaffold Architectures for Tissue Engineering Applications. *Biomaterials* **2002**, *23*, 1169−1185.

(9) Woodfield, T. B. F.; Malda, J.; de Wijn, J.; Peters, F.; Riesle, J.; van Blitterswijk, C. A. Design of Porous Scaffolds for Cartilage Tissue Engineering Using a Three-Dimensional Fiber-Deposition Technique. *Biomaterials* **2004**, *25*, 4149−4161.

(10) Williams, J. M.; Adewunmi, A.; Schek, R. M.; Flanagan, C. L.; Krebsbach, P. H.; Feinberg, S. E.; Hollister, S. J.; Das, S. Bone Tissue Engineering Using Polycaprolactone Scaffolds Fabricated via Selective Laser Sintering. *Biomaterials* **2005**, *26*, 4817−4827.

(11) Tan, K. H.; Chua, C. K.; Leong, K. F.; Cheah, C. M.; Cheang, P.; Abu Bakar, M. S.; Cha, S. W. Scaffold Development Using Selective Laser Sintering of Polyetheretherketone-Hydroxyapatite Biocomposite Blends. *Biomaterials* **2003**, *24*, 3115−3123.

(12) Pati, F.; Gantelius, J.; Svahn, H. A. 3D Bioprinting of Tissue/Organ Models. *Angew. Chem., Int. Ed.* **2016**, *55*, 4650−4665.

(13) Murphy, S. V.; Atala, A. 3D Bioprinting of Tissues and Organs. *Nat. Biotechnol.* **2014**, *32*, 773−785.

(14) Vozzi, G.; Previti, A.; De Rossi, D.; Ahluwalia, A. Microsyringe-Based Deposition of Two-Dimensional and Three-Dimensional Polymer Scaffolds with a Well-Defined Geometry for Application to Tissue Engineering. *Tissue Eng.* **2002**, *8*, 1089−1098.

(15) Trachtenberg, J. E.; Mountziaris, P. M.; Miller, J. S.; Wettergreen, M.; Kasper, F. K.; Mikos, A. G. Open-Source Three-Dimensional Printing of Biodegradable Polymer Scaffolds for Tissue Engineering. *J. Biomed. Mater. Res., Part A* **2014**, *102*, 4326−4335.

(16) Meulenbroek, B.; Storm, C.; Bertola, V.; Wagner, C.; Bonn, D.; van Saarloos, W. Intrinsic Route to Melt Fracture in Polymer Extrusion: A Weakly Nonlinear Subcritical Instability of Viscoelastic Poiseuille Flow. *Phys. Rev. Lett.* **2003**, *90*, No. 024502.

(17) Nemir, S.; West, J. L. Synthetic Materials in the Study of Cell Response to Substrate Rigidity. *Ann. Biomed. Eng.* **2010**, *38*, 2−20.

(18) Kim, H. N.; Kang, D. H.; Kim, M. S.; Jiao, A.; Kim, D. H.; Suh, K. Y. Patterning Methods for Polymers in Cell and Tissue Engineering. *Ann. Biomed. Eng.* **2012**, *40*, 1339−1355.

(19) Sachlos, E.; Czernuszka, J. T. Making Tissue Engineering Scaffolds Work. Review: The Application of Solid Freeform Fabrication Technology to the Production of Tissue Engineering Scaffolds. *Eur. Cells Mater.* **2003**, *5*, 29−39.

(20) Miyazawa, M.; Torii, T.; Toshimitsu, Y.; Okada, K.; Koyama, I.; Ikada, Y. A Tissue-Engineered Artificial Bile Duct Grown to Resemble the Native Bile Duct. *Am. J. Transplant.* **2005**, *5*, 1541−1547.

(21) Tocchi, A.; Mazzoni, G.; Liotta, G.; Lepre, L.; Cassini, D.; Miccini, M. Late Development of Bile Duct Cancer in Patients Who Had Biliary-Enteric Drainage for Benign Disease: A Follow-Up Study of More than 1,000 Patients. *Ann. Surg.* **2001**, *234*, 210−214.

(22) Aikawa, M.; Miyazawa, M.; Okamoto, K.; Toshimitsu, Y.; Torii, T.; Okada, K.; Akimoto, N.; Ohtani, Y.; Koyama, I.; Yoshito, I. A Novel Treatment for Bile Duct Injury with a Tissue-Engineered Bioabsorbable Polymer Patch. *Surgery* **2010**, *147*, 575−580.

(23) Miyazawa, M.; Aikawa, M.; Okada, K.; Toshimitsu, Y.; Okamoto, K.; Koyama, I.; Ikada, Y. Regeneration of Extrahepatic Bile Ducts by Tissue Engineering with a Bioabsorbable Polymer. *J. Artif. Organs* **2012**, *15*, 26−31.

(24) Aikawa, M.; Miyazawa, M.; Okamoto, K.; Toshimitsu, Y.; Okada, K.; Akimoto, N.; Ueno, Y.; Koyama, I.; Ikada, Y. An Extrahepatic Bile Duct Grafting Using a Bioabsorbable Polymer Tube. *J. Gastrointest. Surg.* **2012**, *16*, 529−534.

(25) Thrimurthulu, K.; Pandey, P. M.; Reddy, N. V. Optimum Part Deposition Orientation in Fused Deposition Modeling. *Int. J. Mach. Tools Manuf.* **2004**, *44*, 585−594.

(26) Peltola, S. M.; Melchels, F. P. W.; Grijpma, D. W.; Kellomaki, M. A Review of Rapid Prototyping Techniques for Tissue Engineering Purposes. *Ann. Med.* **2008**, *40*, 268−280.

(27) Wang, S.; Zeng, C. C.; Lai, S. Y.; Juang, Y. J.; Yang, Y.; Lee, L. J. Polymeric Nanonozzle Array Fabricated by Sacrificial Template Imprinting. *Adv. Mater.* **2005**, *17*, 1182−1186.

(28) Azam, A.; Laflin, K. E.; Jamal, M.; Fernandes, R.; Gracias, D. H. Self-Folding Micropatterned Polymeric Containers. *Biomed. Microdevices* **2011**, *13*, 51−58.

(29) Bassik, N.; Stern, G. M.; Jamal, M.; Gracias, D. H. Patterning Thin Film Mechanical Properties to Drive Assembly of Complex 3D Structures. *Adv. Mater.* **2008**, *20*, 4760−4764.

(30) Yimsiri, P.; Mackley, M. R. Spin and Dip Coating of Light-Emitting Polymer Solutions: Matching Experiment with Modelling. *Chem. Eng. Sci.* **2006**, *61*, 3496−3505.

(31) Kang, T. Y.; Lee, J. H.; Kim, B. J.; Kang, J. A.; Hong, J. M.; Kim, B. S.; Cha, H. J.; Rhie, H. J.; Cho, D. W. In vivo endothelization of tubular vascular grafts through in situ recruitment of endothelial and endothelial progenitor cells by RGD- fused mussel adhesive proteins. *Biofabrication* **2015**, *7*, No. 015007.

DOI: 10.1021/acsami.7b00849
ACS Appl. Mater. Interfaces 2017, 9, 12290−12298

(32) Hunt, D. R.; Scott, A. J. Changes in Bile Duct Diameter after Cholecystectomy: A 5-year Prospective Study. *Gastroenterology* **1989**, *97*, 1485−1488.
(33) Li, Q.; Tao, L.; Chen, B.; Ren, H. Z.; Hou, X. L.; Zhou, S. Q.; Zhou, J. X.; Sun, X. T.; Dai, J. W.; Ding, Y. T. Extrahepatic Bile Duct Regeneration in Pigs Using Collagen Scaffolds Loaded with Human Collagen-Binding bFGF. *Biomaterials* **2012**, *33*, 4298−4308.
(34) Zong, C.; Wang, M.; Yang, F.; Chen, G.; Chen, J.; Tang, Z.; Liu, Q.; Gao, C.; Ma, L.; Wang, J. A Novel Therapy Strategy for Bile Duct Repair Using Tissue Engineering Technique: PCL/PLGA Bilayered Scaffold with hMSCs. *J. Tissue Eng. Regener. Med.* **2015**, *3*, 579−589.

DOI: 10.1021/acsami.7b00849
ACS Appl. Mater. Interfaces 2017, 9, 12290−12298